8-9-2006

Steady State and Transient Dynamical Systems Analysis of Uncoupled Roll Response for a Traditional Versus Advanced Hull Form

Sarah Eileen Juckett

University of New Orleans

Steady State and Transient Dynamical Systems Analysis of Uncoupled Roll Response for a Traditional Versus Advanced Hull Form

A Thesis

Submitted to the Graduate Faculty of the
University of New Orleans
in partial fulfillment of the
requirement for the degree of

Master of Science
in
Engineering
with concentration in
Naval Architecture and Marine Engineering

By

Sarah Eileen Juckett

B.S., United States Coast Guard Academy, 1999

August 2006

DEDICATION

This work is dedicated to my family: My ever loving, ever patient husband Paul Crigler who supported me always, and my parents Rosemary and Donald and my sister Karen who cheered me on to the finish. Thank you.

ACKNOWLEDGEMENT

Special thanks to the thesis committee chair Dr. J. Falzarano for his guidance and encouragement and the committee members, Dr. W. Vorus and Dr. L. Birk, for their interest in this project. Also, to Srinivas Vishnubhotla who was always there to answer questions.

TABLE OF CONTENTS

LIST OF FIGURES

LIST OF TABLES

1. INTRODUCTION

1.1 Motivation

The two ships represented in this thesis are dramatically different in design, but both exhibit similar properties such as length and breadth. The traditional hull form is represented by a typical flare-sided design with a forward reaching bow while the advanced hull form has a modified tumblehome and a truncated bow. The difference in shapes provides an interesting problem, comparing the roll responses for these two very different vessels while keeping certain shape parameters such as length, beam, and draft constant.

1.2 Previous Work

The steady state and transient techniques used in this thesis have been extensively used in the past to predict the complicated dynamics of sea going vessels. These dynamics exist for the specific situation where the system stability is degraded to the point that capsizing might occur, however that is realized (water on deck, icing, dangerous loading condition or a combination of the above). These techniques have been used to model the capsizing dynamics of a small fishing vessel [6] and extended to multiple degrees of freedom with large amplitude forcing [5]. The same techniques were used to examine the United States Navy's T-AGOS ocean survey vessel for large amplitude rolling motion [4] and for a complete six degrees of freedom T-AGOS study [8] and [12]. The wave amplitudes were then varied and the progressive transient sampling was then compared [3]. The steady state and transient study was then extended to floating offshore platform rolling motions [10].

The single degree of freedom for this traditional hull form was first explored in 2005 in [9] and continued in [11]. This thesis is limited to the one degree of freedom case of roll and roll responses.

1.3 Non-linearity, Stability and Chaos

Linear approximation of systems are often sufficient but limited ways to understand the dynamics of that system. However, sometimes non-linear effects cannot be neglected and modeling systems with non-linearity better represents the actual dynamics [18]. Non-linear terms can be found in any component of the equations of motion: inertial and dissipative terms, as well as restoring and external forces, and also in the boundary conditions [18]. In a dynamical system with varied parameters, steady state solutions may be stable or unstable. Steady state roll responses model a softening spring of a pendulum system, where the amplitude A is a function of the encounter frequency ω_e. For certain values of the encounter frequency there are multiple solutions. Where multiple solution exists, two are stable solutions and one is unstable [18]. The sudden change observed in the magnification curve is called a bifurcation. The transient response will be influenced by the unstable solution repelling nearby states [18]. In non-linear systems, the initial conditions influence which solution will be observed in experiments [18]. Motion is represented in transient responses in the Poincaré map. With the Poincaré mapping, different kinds of periodic motion and manifold intersections that may lead to chaos can be distinguished [18]. These concepts will be explored further in the appendices.

1.4 Ship Comparisons

The United States Navy's newest design for a guided missile destroyer, the DDX or the DDG-1000 ZUMWALT class, is dramatically different than a traditional destroyer. The distinctive changes are reflected in the modified tumblehome and truncated bow. Compared

to the most recent counterpart, the DDG-51 has a traditional flare-sided design and forward reaching bow. Here the traditional hull form is represented by the DDG-51 and the advanced hull form is represented by the DDG-1000. The Office of Naval Research (ONR) has published representative ship plans for both the DDG-51 and the DDG-1000. By selecting comparative righting arm curves it is possible to examine a system that may be characteristically unstable. Several modeled conditions are represented in this thesis. The first is a low damping case for each ship and the second is a high damping case for each ship. The extreme steady state cases are identified and corresponding transient movement is mapped.

2. SHIP CHARACTERISTICS

In this chapter, the defining ship characteristics will be described in detail. These are not the actual dimensions of the naval vessels, just representative plans.

2.1 Hull Form Comparison

The body plans for both ships are included in order to visualize the differences in the two hull forms. Below is the traditional hull form used or the DDG-51, Aegis class.

Fig. 2.1: Traditional Hull Form Body Plan

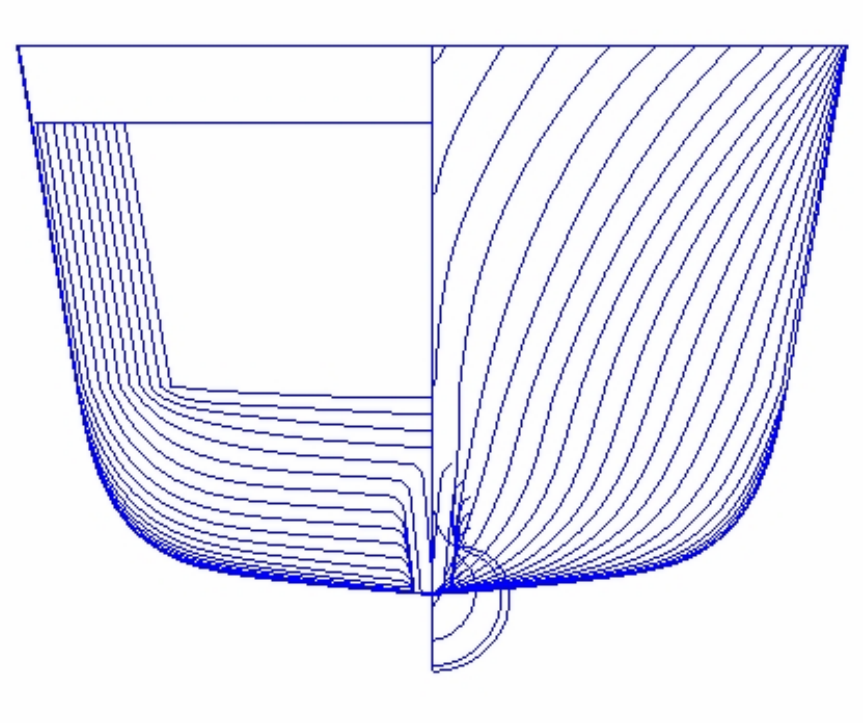

The advanced hull form lines are representative of the DDG-1000. The modified tumblehome is apparent from the body plan.

Fig. 2.2: Advanced Hull Form Body Plan

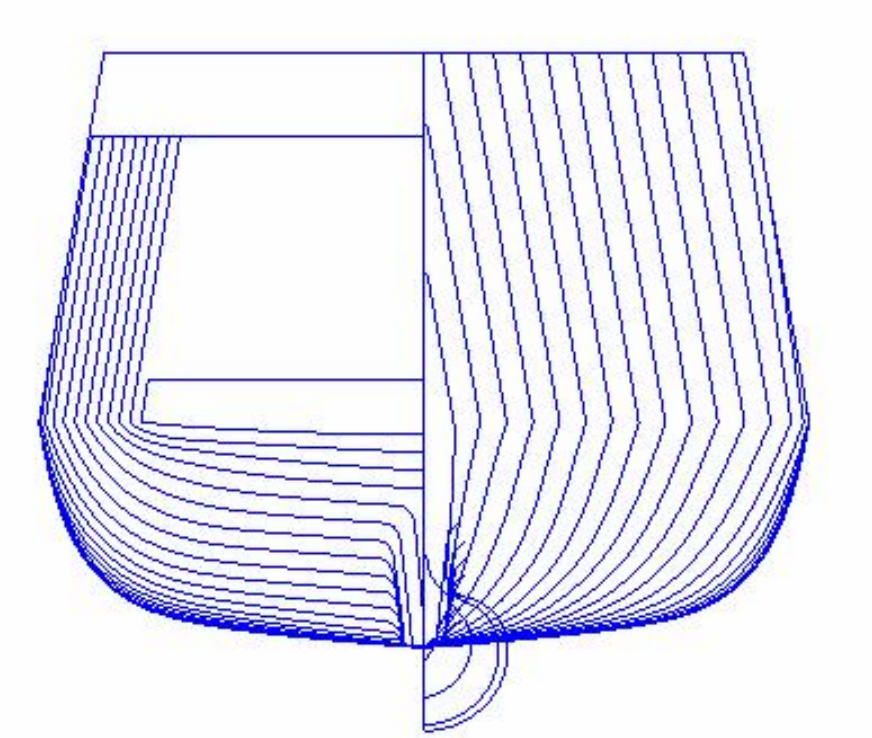

Fig. 2.3: Traditional Hull Form Profile Plan

The bow sections are best viewed by the profile plan. Both ships exhibit a modern surface combatant-type underbody and sonar dome. Statistics from the Office of Naval Research describe both forms as having a displacement of 8,790 tonnes (8,651 long tons), with a length of 154 meters (505 feet), a beam of 18.8 meters (61.7 feet) and a design draft of 5.5 meters (18 feet) [2].

Fig. 2.4: Advanced Hull Form Profile Plan

2.2 Righting Arm Curves

The conditions for the righting arm curves were derived from two different sources. The traditional righting arm curve was developed with the program STAAF and the advanced righting arm curve was developed from ONR data [2] and a third order curve fit was constructed. The transverse metacentric height (GM_T) for the traditional righting arm curve was 2.0 meters (6.56 feet) and the advanced righting arm curve was 2.01 meters (6.59 feet). The limiting GM_T for the traditional hull form is 0.19 meters (0.62 feet) and the limiting righting arm for the advanced hull form is the one used above, 2.01 meters (6.59 feet). At a preliminary glance, the traditional hull form case already has a greater static stability. The angle of vanishing stability for both ships was 1.44 radians. These righting arm curve equations are used in the restoring force portion of the roll equation and account for a portion of the non-linearity of the system. The heel angle is denoted by ϕ.

Tab. 2.1: Transverse GM Limits (Sarchin and Goldberg Criteria)

Ship	GM_T Meters	GM_T Feet
Traditional	0.19 m	0.62 ft
Advanced	2.01 m	6.59 ft

Tab. 2.2: Approximated Third Order Righting Arm Curve Equations

Ship	Third Order Approximation
Traditional	$6.56\phi - 3.12\phi^3$
Advanced	$3.58\phi - 1.73\phi^3$

Fig. 2.5: Limiting Righting Arm Curves Office of Naval Research Data

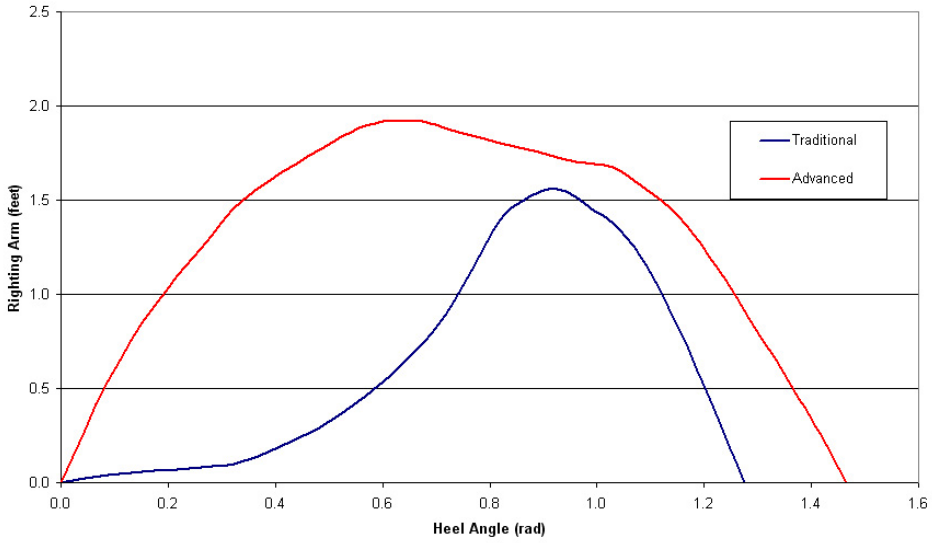

Fig. 2.6: Traditional Hull Form Righting Arm Curve Approximation

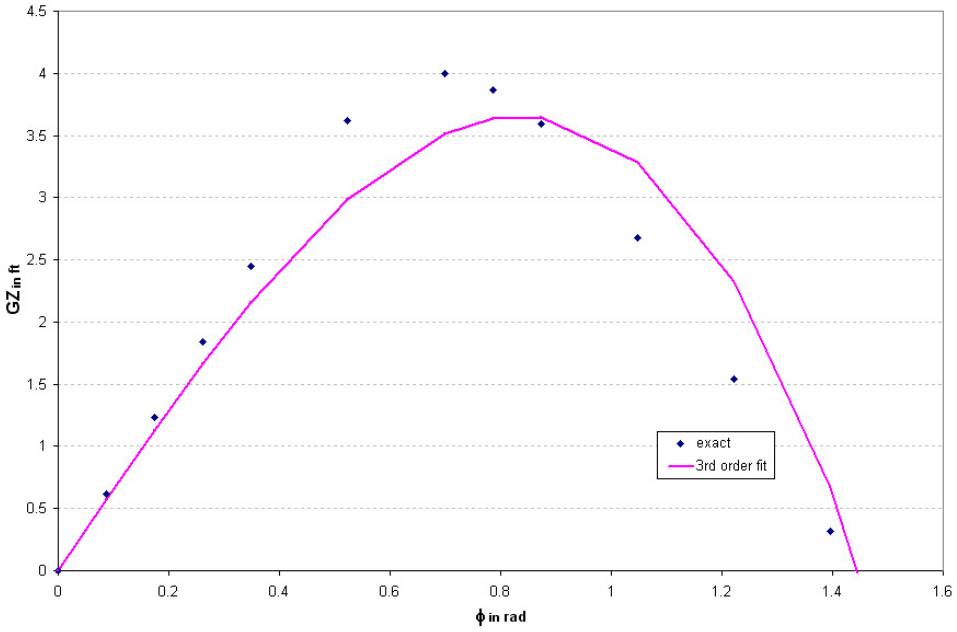

Fig. 2.7: Advanced Hull Form Righting Arm Curve Approximation

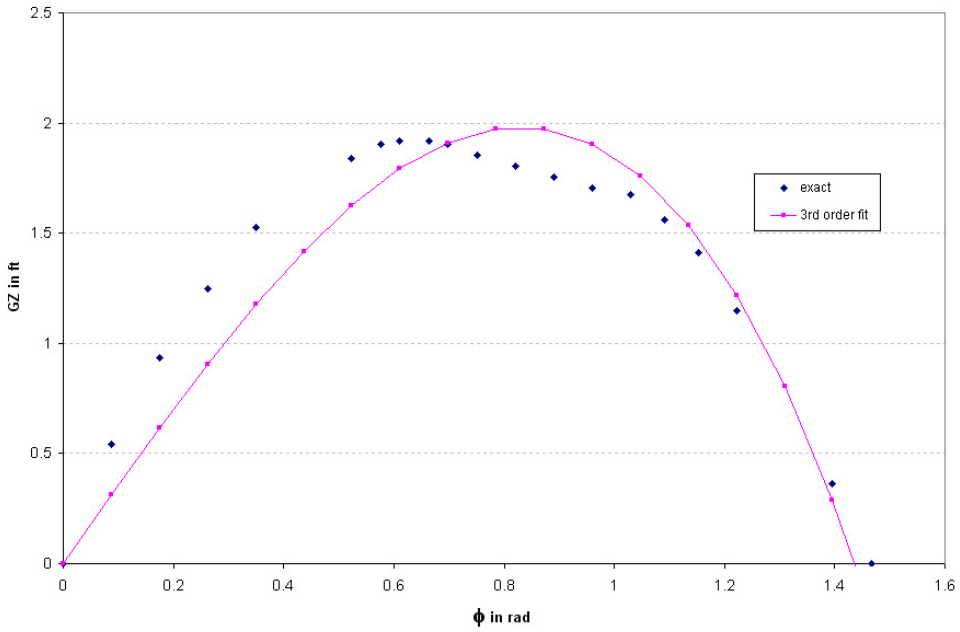

3. ROLL MOTIONS

Even though roll motions are strongly coupled with sway and yaw, examining roll by itself is necessary to pinpoint that extreme motion. Roll motions are difficult to predict for several reasons. They are complicated near roll resonance and cause typical ship forms to roll severely. With large roll angles, there are strong non-linearities occurring in the hydrodynamic damping and possibly in the static roll restoring moment [16]. Within this study the roll non-linearities are approximated by using linear coefficients which depend on the amplitude of the resulting motion and the ship's forward speed [16]. Isolating the effects of roll motion for a zero forward speed case is accomplished by changing the existing coordinate system. This is done by rotating the axes through an angle $\hat{\psi}$ about the y axis and selecting $\hat{x}$ and $\hat{z}$ so that $\hat{I}_{42} + \hat{A}_{42} = 0$ and $\hat{I}_{62} + \hat{A}_{62} = 0$. The angle $\hat{\psi}$ is also picked so that $\hat{I}_{46} + \hat{A}_{46} = 0$ and the $C^*_{44}(|\bar{\eta}_4|)$ is approximated by $\Delta g \cdot \bar{G}\bar{M}_T$) [16]. The new roll equation of motion becomes:

$$[-\omega_e^2(\hat{I}_{44} + \hat{A}_{44}) + i\omega_e \hat{B}^*_{44} + C^*_{44}]\bar{\eta}_4 + \hat{B}_{42}\bar{\eta}_2 + \hat{B}_{46}\bar{\eta}_6 = \hat{F}_4$$

With these changes roll is now only coupled through $\hat{B}_{42}$ and $\hat{B}_{46}$ [16]. In order to have a pure roll equation of motion, these coupling terms are ignored. The above uncoupled roll equation assumes that the center of the coordinate system is the roll center and that a different roll center may be required for each frequency [16].

3.1 Damping Approximations

The quadratic damping portion of the inputs were developed from sallying experiments conducted in model tests. Two cases were used, one where the rudders are at zero (0) degrees and one where the rudders are at an exaggerated angle, ninety (90) degrees. The two cases correspond to a high damping case (maximizing the rudder profile) and a low damping case (minimizing the rudder profile). These two rudder positions are referred to as the high damping and low damping cases in the following sections.

3.2 Approximated Equations

The ship motions program SHIPMO developed by Robert F. Beck [1] was used to determine the components for the equation of motion. The initial conditions were given for each ship with the program calculating responses for thirteen (13) wave angles with a ship speed of sixteen (16.0) feet per second or approximately nine and a half (9.5) knots. The wave frequency was 0.5 radians per second. SHIPMO gave hydrostatic results for displacement and coefficients for each of the encounter frequencies ω_e.

Tab. 3.1: Ship Displacements

Ship	Displacement
Traditional	8215.2 LT
Advanced	8900.3 LT

Tab. 3.2: Roll Inertia for Traditional and Advanced Hull

Traditional I_{44}	$2.74e^8$
Advanced I_{44}	$2.82e^8$

The exciting force F_4, added mass A_{44}, inertia I_{44} and damping B_{44} coefficients were calculated for both the traditional and advanced hull form. The data extracted from the ship motions program was compiled for the range of encounter frequencies from approximately

$\omega_e = 0.37$ to $\omega_e = 0.62$ radians per second. The range of encounter frequencies corresponds to the ships turning at a steady speed of ten (10) knots with a heading angle varying from zero (0) degrees to one hundred and eighty (180) degrees. The data was curve fit to compile equations to describe the previously mentioned coefficients for the encounter frequency range. Those equations are listed below.

Tab. 3.3: Added Mass Coefficients for Traditional and Advanced Hull Forms

Traditional A_{44}	$-6.02e^7\omega_e^3 + 7.76e^8\omega_e^2 - 2.92e^8\omega_e + 1.15e^8$
Advanced A_{44}	$-8.41e^7\omega_e^2 + 9.61e^7\omega_e + 4.91e^7$

Tab. 3.4: Damping Coefficients for Traditional and Advanced Hull Forms

Traditional B_{44}	$1.69e^8\omega_e^3 - 8.63e^7\omega_e^2 + 1.32e^7\omega_e - 2.46e^5$
Advanced B_{44}	$9.10e^7\omega_e^2 - 5.60e^7\omega_e + 9.27e^6$

Tab. 3.5: Roll Exciting Force for Traditional and Advanced Hull Forms

Traditional F_4	$-4.70e^9\omega_e^4 + 9.32e^9\omega_e^3 - 6.97e^9\omega_e^2 + 2.33e^9\omega_e - 2.92e^8$
Advanced F_4	$-4.31e^9\omega_e^4 + 8.53e^9\omega_e^3 - 6.36e^9\omega_e^2 + 2.12e^9\omega_e - 2.65e^8$

4. STEADY STATE MAGNIFICATION CURVES

4.1 Forcing and Damping

The two significant variables for these experiments are the damping and the forcing. The low and high damping cases have been discused in the previous chapter. The forcing representing the combination of the Froude-Krylov and Diffraction forces varied wave amplitudes from one (1.0) foot to five (5.0) feet.

4.2 Comparisons

With linear responses, the maximum response is often close to the resonance frequency. With non-linear responses, the effect of nonlinear damping and restoring may change the peak roll amplitude. Depending on the restoring spring, whether softening or hardening, the peak amplitude may occur at a higher or lower frequency as explained in Appendix C. The first figure in this chapter represents the traditional hull form with low damping and full wave amplitude range. The peak amplitude for the eight foot and the ten foot wave is at a significantly higher frequency than the resonance frequency of 0.5 radians per second. The encounter frequency of the two highest wave amplitudes are at a higher frequency than the resonance frequency of 0.5 radians per second and the two lowest wave amplitudes are at a lower frequency than the resonance frequency. The peak amplitude for the five foot wave amplitude is also extremely close to the 1.44 radians of vanishing stability.

Tab. 4.1: Peak Wave Height vs. Encounter Frequency, Traditional Hull Form (Low Damping Case)

Wave Height	Encounter Frequency	Roll Amplitude
2 feet	.57 rad/s	0.23 rad
4 feet	.55 rad/s	0.52 rad
8 feet	.41 rad/s	1.36 rad
10 feet	.39 rad/s	1.42 rad

Fig. 4.1: Traditional Roll Response vs. Encounter Frequency Low Damping Case

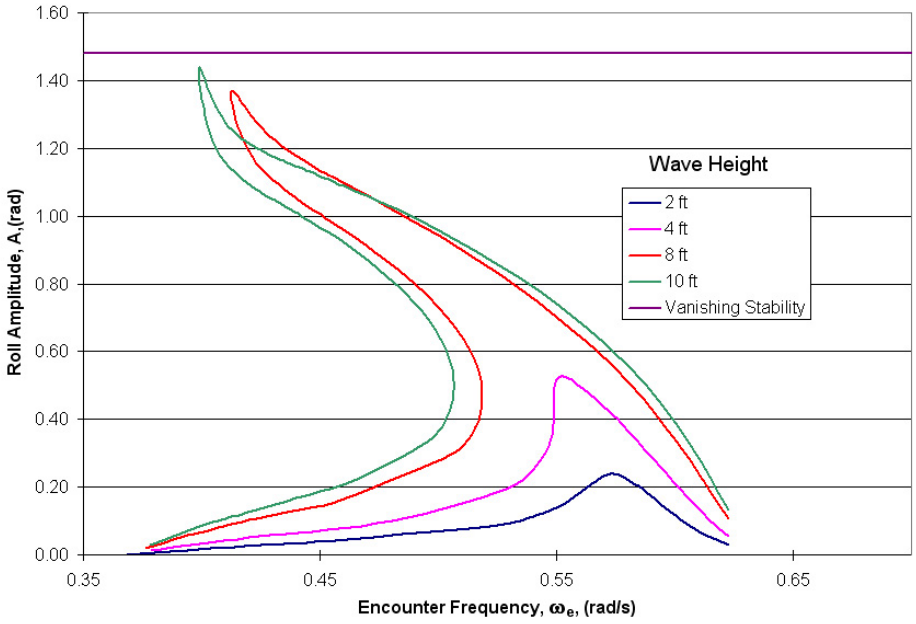

Examining the difference between the low and the high damping case responses reveals an increase in the damping the corresponding peak roll amplitudes all are at a lower frequency than the resonance frequency of 0.5 radians per second. The high damping case also exhibited a wide region of multivaluedness for the two highest wave amplitudes as compared to the low damping case.

The advanced hull form responses in the low damping case shows a significant change where all the peak amplitudes moved for all of the forcing cases, including the lower wave amplitudes. All of the encounter frequencies are higher than the resonance frequency of 0.5 radians per second.

Fig. 4.2: Traditional Roll Response vs. Encounter Frequency High Damping Case

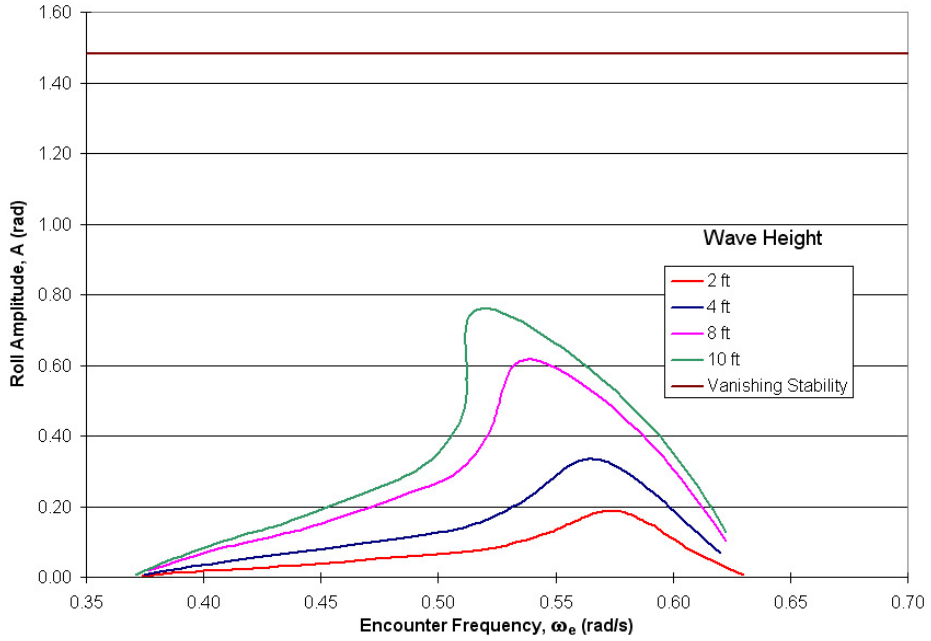

Tab. 4.2: Peak Wave Height vs. Encounter Frequency, Traditional Hull Form (High Damping Case)

Wave Height	Encounter Frequency	Roll Amplitude
2 feet	.57 rad/s	0.18 rad
4 feet	.56 rad/s	0.33 rad
8 feet	.53 rad/s	0.61 rad
10 feet	.51 rad/s	0.75 rad

Again, for the advanced hull form high damping case, all the encounter frequencies for the peak roll amplitude fell at higher frequencies than at the resonance frequency of 0.5 radians per second

For the low damping (worst case) the traditional hull form's peak roll amplitudes were higher at five (5) foot and four (4) foot wave amplitudes, but the advanced hull form low wave amplitude roll responses were higher than the traditional hull form roll responses.

The comparison between the two low damping cases of the traditional and advanced hull form show a greater roll amplitude much closer to the angle of vanishing stability for the traditional case and a broader range of multivaluedness for the traditional case than

Tab. 4.3: Peak Wave Height vs. Encounter Frequency, Advanced Hull Form (Low Damping Case)

Wave Height	Encounter Frequency	Roll Amplitude
2 feet	.415 rad/s	0.61 rad
4 feet	.384 rad/s	0.81 rad
6 feet	.385 rad/s	0.87 rad
8 feet	.383 rad/s	0.90 rad
10 feet	.380 rad/s	0.93 rad

Tab. 4.4: Peak Wave Height vs. Encounter Frequency, Advanced Hull Form (High Damping Case)

Wave Height	Encounter Frequency	Roll Amplitude
2 feet	.438 rad/s	0.31 rad
4 feet	.430 rad/s	0.46 rad
6 feet	.422 rad/s	0.57 rad
8 feet	.417 rad/s	0.65 rad
10 feet	.410 rad/s	0.72 rad

the advanced case. Both the traditional and advanced hull forms show the marked distance between the peak roll amplitude encounter frequencies and the resonance frequency. The results for the low damping case with the highest wave amplitude of five (5.0) feet for the magnification curves alone show that the highest (worst case) roll amplitudes occur for the traditional hull form. However, the Poincaré maps for each of the traditional and advanced hull form at the highest wave amplitude show a different global picture.

Fig. 4.3: Advanced Roll Response vs. Encounter Frequency Low Damping Case

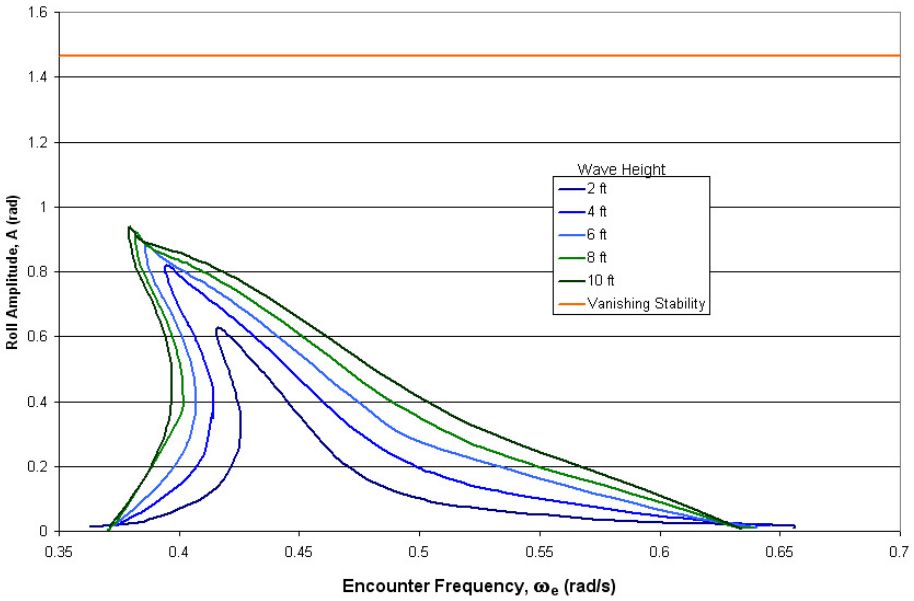

Fig. 4.4: Advanced Roll Response vs. Encounter Frequency High Damping Case

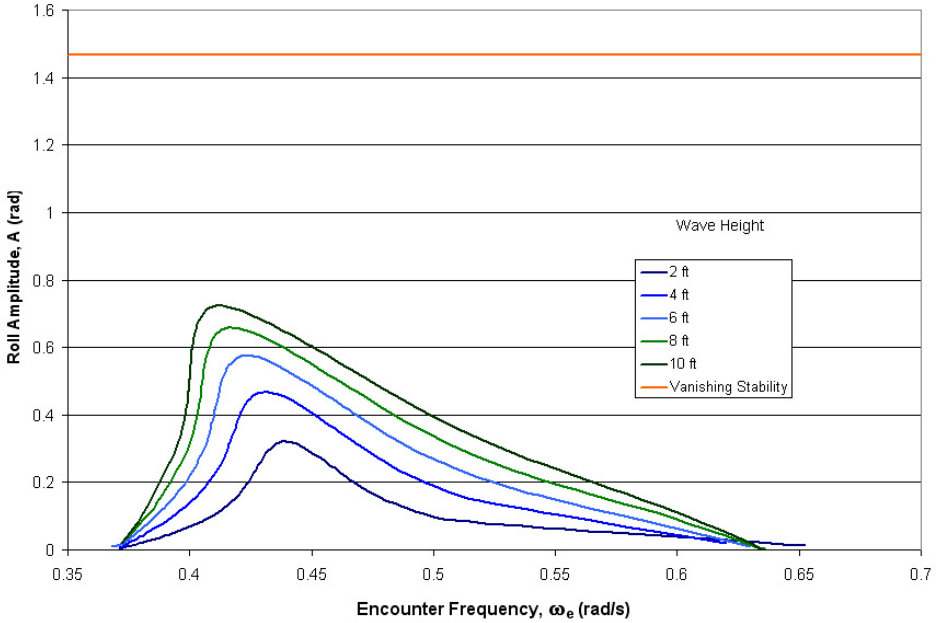

5. TRANSIENT SAMPLING

5.1 Poincaré Maps

The transient sampling for the Poincaré maps shows a different dynamic picture than the magnification curves for the same system parameters. For a given encounter frequency ω_e, the roll velocity can be compared to the roll amplitude over time and a global picture for that ω_e is developed. The stable and unstable solutions are pinpointed, and by identifying the initial conditions, the attraction to a specific solution (whether stable or unstable) is shown.

5.2 Frequency Selection and Magnification Curves

The encounter frequencies to examine the Poincaré maps were chosen to be approximately two thirds of the distance from the peak amplitude for each of the traditional and advanced steady state low damping cases. The maximum wave amplitude of five (5) feet was chosen, and the sampling frequencies are given in the following tables.

5.3 Comparisons

The sampling frequencies for traditional and the advanced hull form are taken from the steady state magnification curves. For the region of multivaluedness, there are three solutions, two stable and one unstable. The Poincaré maps identify three important regions of initial conditions surrounding these three solutions.

Fig. 5.1: Traditional Roll Response 10 ft Wave Height Low Damping Case

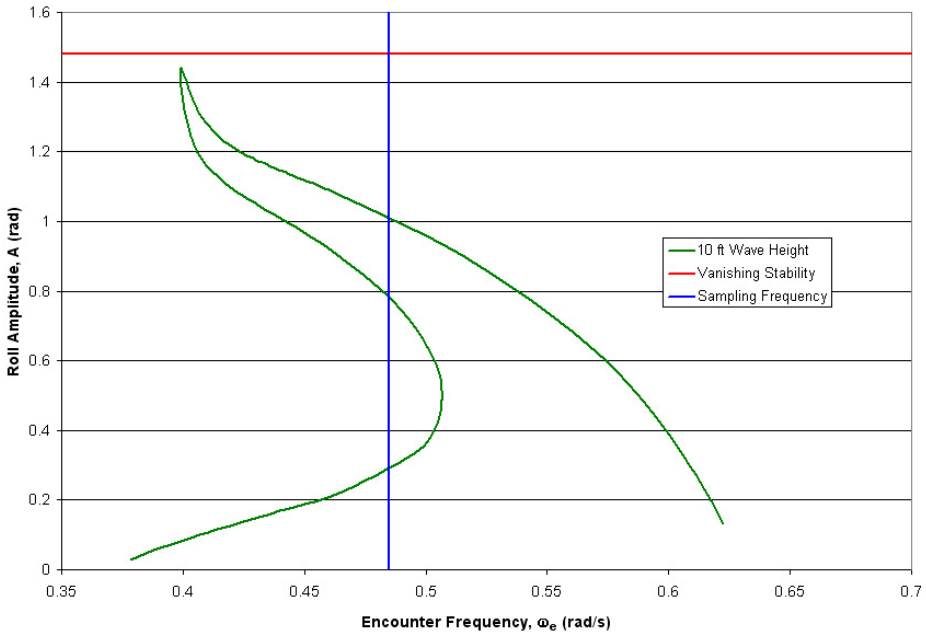

Any point on the map has a corresponding roll amplitude and roll velocity. The points outside of the bounded region are unstable and may lead to capsizing. The points in the bounded region (safe basin) are safe and will be attracted to one of the stable solutions identified by a black dot. The unstable solution is represented by an X. All points in the tear shaped blue curve (or lobe) around the low amplitude stable solution will be attracted to that solution. All other points will be attracted to the high amplitude solution. The unstable solution will repel the trajectory to either stable solution.

Tab. 5.1: Traditional vs. Advanced Poincaré Map Encounter Frequency

Ship	Encounter Frequency
Traditional	.485 rad/s
Advanced	.390 rad/s

Comparing the Poincaré maps show that for the traditional hull form the regions of safe basin in the transient sampling map area is greater, so a greater percentage of initial conditions stay within this safe basin. However, the magnification curves showed the roll

Fig. 5.2: Advanced Roll Response 10 ft Wave Height Low Damping Case

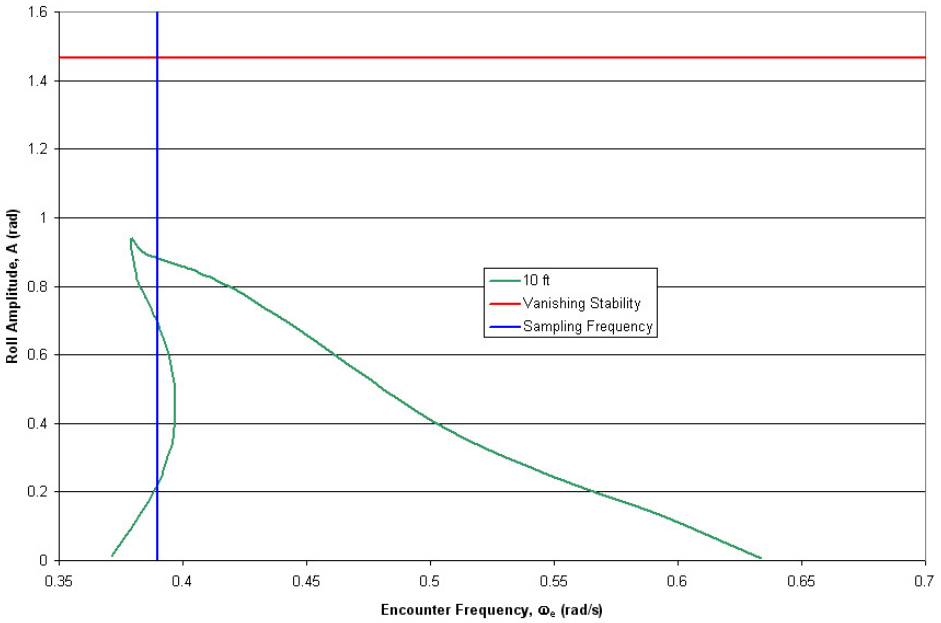

Tab. 5.2: Traditional vs. Advanced Poincaré Map Encounter Frequency Corresponding Steady State Solutions

Ship	High Stable	Unstable	Low Stable
Traditional	1.02 rad	0.75 rad	0.30 rad
Advanced	0.88 rad	0.70 rad	0.23 rad

amplitude is greater and closer to the angle of vanishing stability for the isolated high wave amplitude case for the traditional hull form. Also, the basin of attraction for the low amplitude stable solution for the advanced hull form is an extremely reduced area as compared to the basin of attraction of the traditional hull form.

Fig. 5.3: Traditional Poincaré Map

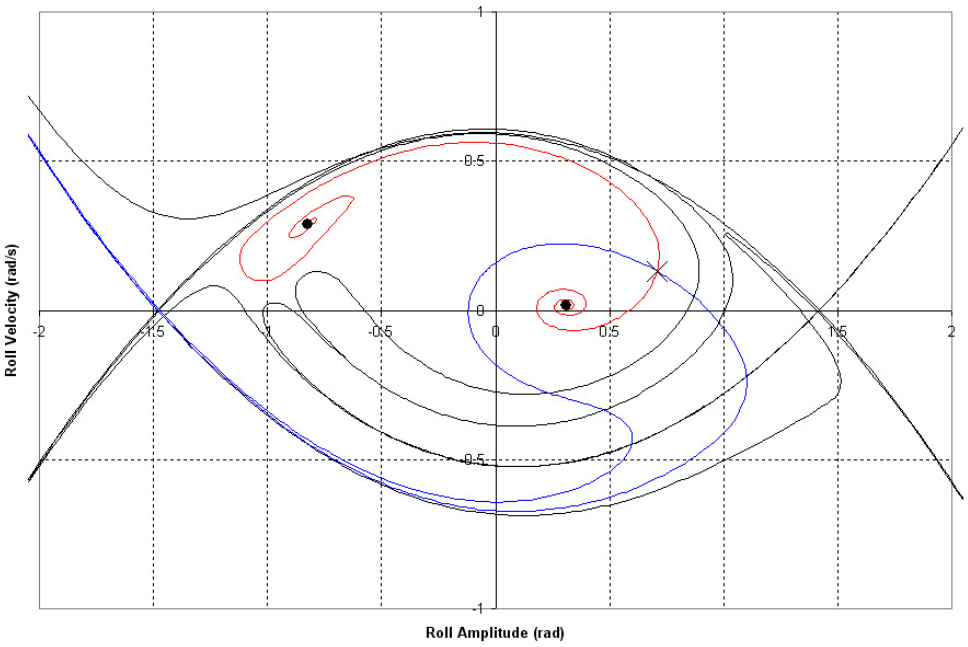

Tab. 5.3: Area Comparison of Safe Basins and Basins of Attractions for the Traditional vs. Advanced Hull Form

Ship	Total Area	Low Stable Basin	Percentage
Traditional	10.92	2.85	26.1%
Advanced	7.06	0.95	13.5%

Fig. 5.4: Advanced Poincaré Map

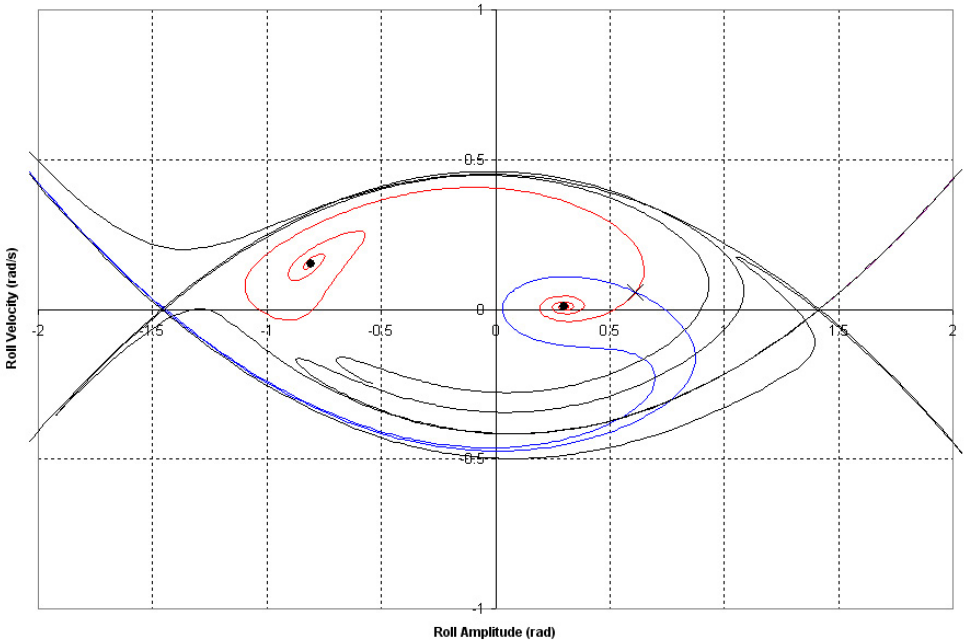

6. CONCLUSIONS

Examining the steady state magnification curves of roll amplitude, the traditional hull form for the low damping case showed the highest roll amplitude closest to the angle of vanishing stability. The traditional hull form encounter frequencies for the higher wave amplitude where higher than resonance and the lower wave amplitudes were at a lower frequency than resonance. The high damping case resulted in the maximum roll amplitudes occurring at lower frequencies than resonance.

The steady state magnification curve of roll amplitude for the advanced hull form for the low and high damping case showed the peak roll amplitudes occurring at higher frequencies than resonance, and the peak roll amplitude for the advanced hull form was less that the traditional for high wave amplitudes but greater for low wave amplitudes for the low damping case.

The Poincaré maps for the high wave amplitude low damping cases for both hull forms showed the safe basins and basins of attraction for the multiple solutions corresponding to the steady state encounter frequencies. Both showed that a higher percentage of initial conditions will attract to the high amplitude steady state stable solution, although the percentage of initial conditions was higher for the advanced hull form.

The safe basin for the traditional hull form was greater in scope than the safe basin for the advanced hull form. The magnification curves show the traditional hull form's roll amplitude at the low damping case was greatest and closest to the angle of vanishing stability.

The associated Poincaré maps show that the initial conditions favor the low roll amplitude steady state solution a greater percentage of the time. The entire initial condition global picture favors the traditional hull form rather than the advanced. Both methods combined provide a better dynamical picture together than when examined separately.

6.1 Applicability

Special attention to the non-linearities in the systems should be paid when examining the frequencies at which the high roll amplitude responses may occur. Also, comparing the transient sampling for the worst case encounter frequency of the steady state magnification curves can broaden the understanding of the system dynamics and the attraction to a particular solution. This examination is not limited to just these two hull forms and can be useful to gain an comprehensive look into a particular ship dynamics problem.

6.2 Future Work

This thesis has only scratched the surface with regards to a comprehensive look at these two hull forms. A greater range of frequencies and sea states as well as more model tests are needed to give a robust examination of this comparison problem. Different combinations of these techniques should be employed, such as comparing the Poincaré maps for the same wave amplitude and different encounter frequencies as well as comparing the Poincaré maps for the same encounter frequency but a range of wave amplitudes to better understand the changing steady state and transient dynamics of the given system. After the complete one degree of freedom case is completed, then multiple (three or six) degree of freedom cases should be utilized and compared.

7. APPENDIX A: EQUATIONS OF MOTION AND SHIPMO

The six degrees of freedom are surge, sway, heave, roll, pitch and yaw. Translation in the X direction is η_1, surge and the moment about the X axis is η_4, roll. Translation in the Y direction is η_2, sway and the moment about the Y axis is η_5, pitch. Translation in the Z direction is η_3, heave and the moment about the Z axis is η_6, yaw [16]. The three axis fixed system of x_o, y_o and z_o are translated to the ship system moving at a constant velocity U_o by

$$x_o = x + U_o t$$

$$y_o = y$$

$$z_o = z$$

Where t is time [16]. The relative orientation of $\bar{x}, \bar{y}$ and $\bar{z}$ to x, y, and z determine the ship motions [16]. The linearized equations of motion for an unrestrained vessel in sinusoidal waves are

$$\sum_{k=1}^{6} [-\omega_e^2(\Delta_{jk} + A_{jk}) + i\omega_e B_{jk} + C_{jk}]\,\bar{\eta}_k = F_j^I + F_j^D$$

where $j = 1, 2, \ldots, 6$[16]The components of the above equation are the frequency of wave encounter, ω_e is

$$\omega_e = \omega_o - \frac{\omega_o^2}{g} U_o cos\mu$$

Where μ is the angle between ship heading and wave heading [16]. The mass matrix, Δ_{jk} is as follows:

$$\Delta_{jk} = \begin{vmatrix} \Delta & 0 & 0 & 0 & +\Delta\bar{z}_c & 0 \\ 0 & \Delta & 0 & -\Delta\bar{z}_c & 0 & +\Delta\bar{x}_c \\ 0 & 0 & \Delta & 0 & -\Delta\bar{x}_c & 0 \\ 0 & -\Delta\bar{z}_c & 0 & I_{44} & 0 & -I_{46} \\ +\Delta\bar{z}_c & 0 & -\Delta\bar{x}_c & 0 & I_{55} & 0 \\ 0 & +\Delta\bar{x}_c & 0 & -I_{46} & 0 & I_{66} \end{vmatrix}$$

where $\bar{x}_c$ and $\bar{z}_c$ are the coordinates of the center of gravity of the ship [16]. A_{jk} is the added mass in the j^{th} mode due to the unit motion is the k^{th} direction, B_{jk} is the damping coefficient in the j^{th} mode due to unit motion in the k^{th}direction and C_{kj} is the hydrostatic restoring force coefficient in the j^{th} mode due to motion in the k^{th} direction [16]. The hydrostatic restoring force is zero with the exception of the following terms: C_{33}, $C_{35} = C_{53}$, C_{44}, and C_{55} [16]. The exciting force components F_j^I and F_j^D are the Froude-Krylov exciting force and the diffraction exciting force. The ship motions program SHIPMO uses damping coefficients developed in [7]. It is an experimental compilation of hull forms that may not include these advanced and traditional hull forms in accurate quadratic damping. Only linear damping is taken from the computer program and quadratic damping is derived from experiments.

8. APPENDIX B: BIFURCATION AND BIFPACK

To examine if the dynamical systems represented are stable or unstable, with linearizing the stability theory an asymptotic solution to a small initial perturbation is examined. A growing perturbation is unstable, and a decaying perturbation is stable [13]. The steady state magnification curves contain regular turning points, which are points which the curve changes signs and the forcing function does not equal zero [13]. The Factorization Theorem in One Dimension implies that the curve is stable on one side of a regular turning point (also called a saddle-node) and unstable one the other side [13]. The computer program BIFPACK was developed by R. Seydel and is a set of Fortran codes that can calculate the parameter dependence of ordinary differential equations [17]. The main parameter, λ, is the branching parameter. Using the package for ordinary differential equations, and the boundary value problem describing the steady state oscillator. The magnification curves are developed from BIFPACK. The equations used are the re-created righting arm curves from ONR [2], the equations developed from SHIPMO, and derivatives of the equations with respect to ω_e which is the branching parameter λ used to track the bifurcation or turning points of the magnification curves in a continuation method.

9. APPENDIX C: SOFTENING SPRING

The nonlinear system of the softening spring is very similar to the magnification curve and the program BIFPACK is used to produce the results. The method of iteration where Duffing's study of the equation

$$m\ddot{x} + c\dot{x} + kx \pm \mu x^3 = Fcos\omega t$$

representing a mass on a cubic spring, excited harmonically with damping. Duffing's steady state harmonic solution without damping with the process of successive approximation is where an assumed solution is substituted into the differential equation. The differential equation is integrated to improve the accuracy [19]. Higher harmonic terms are ignored, and after the second approximation a reasonable solution is obtained. The first assumed solution precedes the undamped equation:

$$x_0 = Acos\omega t$$

$$\ddot{x} + \omega_n^2 x + -\mu x^3 = Fcos\omega t$$

giving the integrated equation solved for ω^2 as

$$\omega^2 = \omega_n^2 \pm \frac{3}{4}\mu A^3 - F$$

When this system is undamped, the amplitude A is discontinuous as it approaches resonance. With the softening spring, as the non-dimensional frequency increases from zero, the amplitude increases and reaches a turning point where the frequency decreases as the amplitude increases, creating a curve that folds back towards zero frequency. It then 'jumps' to a higher amplitude and amplitude diminishes as frequency increases from zero onward. This produces two curves which approach a 'backbone' region asymptotically. The region where there are several solutions for the same ω/ω_n is an unstable region. The unstableness is influenced by both the amount of damping present as well as the rate of change of the forcing [19].

Damping the system changes the curve by eliminating the asymptotic regions and connecting the two curves so the first bends back around to attach to the second at a peak. The differential equation for the softening spring with damping then becomes

$$\ddot{x} + c\dot{x} + \omega_n^2 x - \mu x^3 = Fcos(\omega t + \phi) = A_o cos\omega t - B_o sin\omega t$$

where the magnitude of the force is $F\sqrt{A_o^2 + B_o^2}$. Using the same first approximation as the undamped case, the substitution into the differential equation and integration results in the solutions of

$$A_o = (\omega_n^2 - \omega^2)A + \frac{3}{4}\mu A^3$$

$$B_o = c\omega A$$

The frequency, amplitude and force relationship becomes:

$$F^2 = [(\omega_n^2 - \omega^2)A + \frac{3}{4}\mu A^3]^2 + [c\omega A]^2$$

10. APPENDIX D: POINCARÉ MAPS

The systems described in this thesis are non-autonomous continuous time dynamical systems, and describe a differential equation where the vector field depends on time. For the limit set definitions, a limit set is a set of points in state space that a trajectory repeatedly visits. In [14], some definitions to this problem are examined. A limit set is attracting if there exists an open neighborhood U of set L such that $L(x) = L$ for all $x \in U$. The basin of attraction B_L of an attracting set L is defined as the union of all such neighborhoods U, where B_L is the set of all initial conditions that tend toward L as time progresses to infinity. However, these definitions are related to autonomous, not non-autonomous systems and the limit sets of non-autonomous differential equations are not meaningful unless examined via a Poincaré map [14].

Because the dynamical system studied here may lead to chaos, they exhibit a sensitive dependence on initial conditions. For the specific system, the characteristic trajectories for two initial conditions arbitrarily close to one another diverge until they become uncorrelated [14]. The technique of Poincaré maps transforms a continuous time system into a discrete time system with limits related to the continuous time systems [14]. Points in the Poincaré map may be stable, asymptotically stable, unstable or non-stable. The informal definitions follow where L is defined as stable if all nearby trajectories stay nearby. If the trajectories are attracted, then L is asymptotically stable and if they are repelled, then unstable. For L to be non-stable, at least one trajectory that is not in L is attracted and at least one close trajectory is repelled.

The computer program INSITE [15] and [14] determines the stable and unstable manifolds W^s and W^u of the system. Again, definitions from [14] state that a stable manifold W^s of the limit set L for a flow of ϕ_t are all points of the set whose trajectory $\phi_t(x)$ approaches L as time approaches infinity, and the unstable manifold W^u of the limit set L approaches for the aforementioned flow whose trajectory approaches L as time approaches negative infinity. The stable and unstalbe manifolds are invariant unter ϕ_t. The third order curve fit for the righting arm curves are needed for the Melnikov Method to develop the close form intersecting manifolds of the Poincaré Maps [6].

11. BIBLIOGRAPHY

[1] Beck, Robert F. "Ship Motions" Lecture. Department of Naval Architecture and Marine Engineering. U of Michigan, Ann Arbor. January, 1984.

[2] Belknap, Bill and Brad Campbell. "Office of Naval Research Roll Response Series Hull-forms." Lecture. Naval Surface Warfare Center Seakeeping Division, West Bethesda. 1 December, 2005

[16] Dalzell, John F., Philip Mandel, William C. Webster, Robert F. Beck, William E. Cummings. Principles of Naval Architecture. Rev. 2, Vol. 3. Jersey City: Society of Naval Architects and Marine Engineers, 1989. 41-83

[6] Falzarano, Jeffrey M. "Predicting Complicated Dynamics Leading to Vessel Capsizing." Diss. U of Michigan, 1990.

[12] Falzarano, Jeffrey M., R. Kota and I. Esparza. "A Combined Steady State and Transient Approach to Study Large Amplitude Ship Rolling Motion and Capsizing." Proceedings of the 15th Biennial Conference on Vibrations and Noise Boston: American Society of Mechanical Engineers, 1995. 759-764

[3] Falzarano, Jeffrey M. and R. Kota. "A Combined Steady-state and Transient Approach to Study Extremely Large Amplitude Ship Rolling" EuroMech - 2nd European Nonlinear Oscillations Conference Prague: Euro-Mech, 1996. 53-56

[8] Falzarano, Jeffrey M. and M. Talz Ul Mulk. "Complete Six-Degrees-of-Freedom Nonlinear Ship Rolling Motion." ASME Journal of Offshore Mechanics and Arctic Engineering 116 (1994): 191-201

[4] Falzarano, Jeffrey M. and M. Talz Ul Mulk. "Large Amplitude Rolling Motion of an Ocean Survey Vessel". SNAME Journal of Marine Technology 31 (1994): 278-285

[9] Falzarano, Jeffrey M., S. Vishnubhotla and S. Juckett. "Combined Steady State and Transient Analysis of a Patrol Vessel as Affected by Varying Amounts of Damping and Periodic and Random Wave Excitation" 24th International Conference on Offshore Mechanics and Arctic Engineering Halkidiki: OMAE, 2005.

[11] Falzarano, Jeffrey M., S. Vishnubhotla and S. Juckett. "Steady State and Transient Dynamical Systems Analysis of Uncoupled and Coupled Very Large Amplitude Roll Resone of A Vessel In Regular and Random Waves" 25th International Conference on Offshore Mechanics and Arctic Engineering Hamburg: OMAE, 2006.

[10] Falzarano, Jeffrey M., S. Vishnubhotla and A. Vakakis. "A New Method to Predict Vessel/Platform Critical Dynamics in a Realistic Seaway." Philosophical Transactions of the Royal Society 358 (2000): 1967-1981

[5] Falzarano, Jeffrey M. and Fenglei Zhang. "Multiple Degree of Freedom Global Transient Ship Rolling Motion: Large Amplitude Forcing." ASME Winter Annual Meeting New Orleans: American Society of Mechanical Engineers, 1993. 57-72

[7] Himeno, Yoji. Prediction of Ship Roll Damping - State of the Art. Ann Arbor: U of Michigan, 1981.

[13] Joseph, Daniel D. and Gérard Ioos. Elementary Stability and Bifurcation Theory. 2nd ed. New York: Springer-Verlag, 1980. 1-26

[15] Parker, Thomas S. "INSITE A Software Toolkit for the Analysis of Nonlinear Dynamical Systems." Proceedings of the IEEE 75 (1987): 1081-1089

[14] Parker, Thomas S. and L. O. Chua. Practical Numerical Algorithms for Chaotic Systems. New York: Springer-Verlag, 1989. 1-81

[17] Seydel, R. "Bifpack: A Program Package for Continuation, Bifurcation and Stability Analysis." 1996.

[18] Thomsen, Jon J. Vibrations and Stability: Order and Chaos. London: McGraw Hill, 1997. 63-129

[19] Thomsen, William T. Theory of Vibration with Applications. 5th ed. Upper Saddle River: Prentice Hall, 1998. 436-451

12. VITA

Sarah Eileen Juckett was born in Bartlesville, Oklahoma, and obtained her high school diploma from West Springfield High School (Springfield, Virginia) in 1995. She graduated from the United States Coast Guard Academy (New London, Connecticut) in 1999 with a Bachelor of Science Degree in Naval Architecture and Marine Engineering. She then served as an officer in the United States Coast Guard on the USCGC THETIS, a 270 ft WMEC Coast Guard Cutter in Key West, Florida from 1999 to 2001. She continued to serve in the Coast Guard as a Port Engineer at the Naval Engineering Support Unit in New Orleans, Louisiana until 2003. She is currently employed at Alion Science and Technology in Alexandria, Virginia.